Cite this article
Mohammad N, Meng W, Zhang Y *et al.* (2022)
Desiccation crack formation and prevention in thin bentonite layers.
Environmental Geotechnics **9(8)**: 547–561,
https://doi.org/10.1680/jenge.19.00112

Research Article
Paper 1900112
Received 10/05/2019; Accepted 04/05/2020
Published online 13/11/2021

Keywords: contaminated material/geosynthetics/landfills

Environmental Geotechnics

ice Publishing

Desiccation crack formation and prevention in thin bentonite layers

1 **Noor Mohammad**
School of Civil Engineering, University of Sydney, Sydney, Australia (Orcid:0000-0001-6675-6060)

2 **Weipeng Meng**
Department of Engineering Mechanics, CNMM and AML, Tsinghua University, Beijing, China

3 **Yongmei Zhang**
School of Civil Engineering, University of Sydney, Sydney, Australia

4 **Mingchao Liu**
Mathematical Institute, University of Oxford, Oxford, UK

5 **Abbas El-Zein**
School of Civil Engineering, University of Sydney, Sydney, Australia

6 **Yixiang Gan**
School of Civil Engineering, University of Sydney, Sydney, Australia (corresponding author: yixiang.gan@sydney.edu.au)






Desiccation cracks in clay play an important role in many geoenvironmental applications such as clay liners in engineered landfills, preferential flows and contaminant transport. In this study, a comprehensive series of experiments was conducted to investigate the desiccation cracks due to the combined effects of initial water content and layer thickness on bentonite clay. Slurries of bentonite were prepared with initial water contents ranging from 1200 to 2200%. The slurry was placed in a glass Petri dish and dried at a temperature of 30 ± 2°C. Results from the experiments were illustrated in a phase diagram, and it was found that the interplay between the initial water content and layer thickness has a significant effect on the formation and prevention of desiccation cracks. More specifically, a phase boundary distinguishing between cracked and non-cracked samples was obtained in the constructed phase diagram. A theoretical model based on the critical cracking thickness was developed and then was used to predict this observed phase boundary. Furthermore, a detailed morphology of crack patterns was investigated by employing image analysis techniques followed by statistical analyses. Findings from this study have potential use in clay liner design, where bentonite is used as the main material, as well as in other problems associated with drying soils.

Notation

a_1, a_2	fitting parameters
b_1, b_2	fitting parameters
C	combined material constant
C_f	material constant for fracture
d	specimen characteristic dimension
d_0	reference dimension
E	Young's modulus of clay
E_1'	plane strain elastic modulus
G_{IC}	critical strain-energy release rate
G_s	specific gravity of clay
h	final film thickness of the layer
h_c	critical cracking thickness
K_{IC}	fracture toughness of clay slurry
w	gravimetric water content
w_0	critical (cracking) water content
w_i	initial water content
w_s	mass of the solid (clay) content
w_w	mass of water in the sample
x	observed data
α	slope parameter
λ, λ_0	parameters that can be determined from regression analysis
μ	logarithmic mean of the distribution
ν	Poisson's ratio of clay
ρ_p	clay particle density
ρ_w	density of water
σ^2	logarithmic variance of the distribution
σ_{max}	maximum stress during drying before cracks appear
σ_t	tensile strength of clay
ϕ	particle volume fraction of clay
ϕ_0	average volume fraction
ϕ_i	initial particle volume fraction
Ω	material constant for critical cracking thickness

Introduction

The cracking of clay soils during desiccation is a global issue in many fields of engineering. For example, in geotechnical engineering, soil cracking is a significant problem in roads, earth embankments, slopes and foundations (Li *et al.*, 2009). In agricultural engineering, soil cracks can divert water and act as a major conduit for solute movement in an irrigated land (Bronswijk, 1991). In environmental geotechnics, clay liners underlying sanitary waste landfills are very susceptible to damage due to desiccation cracking (Daniel and Brown, 1987). Clay liners

in landfills damaged as a result of desiccation cracks promote water and leachate migration in surrounding underground soils (Peron *et al*., 2009a). Long-term trends towards drier soils have been documented, likely due to changes in hydrological cycles and higher rates of evapotranspiration, both of which are driven by anthropogenic climate change (e.g. Leao, 2014). Desiccation of clay is hence a critical mechanism through which geotechnical and geoenvironmental structures may experience high vulnerability to climate change (El-Zein, 2016).

Desiccation cracking in clay soils and their consequences have motivated many researchers to investigate crack formation and prevention under various conditions (Colina and Roux, 2000; Costa *et al*., 2013; Khatun *et al*., 2015; Kodikara and Choi, 2006; Lakshmikantha *et al*., 2012; Lau, 1987; Li, 2014; Li and Zhang, 2011; Morris *et al*., 1992; Peron *et al*., 2009a; Shokri *et al*., 2015; Tang *et al*., 2011a; Vogel *et al*., 2005). Several factors affect soil desiccation cracking, such as soil mineral compositions, clay content and soil density (Albrecht and Benson, 2001; da Silva *et al*., 2013; Jayanthi *et al*., 2017; Lu *et al*., 2015; Shinde *et al*., 2012; Tang *et al*., 2008). Meanwhile, natural conditions and physical environments, including soil layer thickness, boundary conditions, temperature and humidity (DeCarlo and Shokri, 2014; Lakshmikantha *et al*., 2018; Tang *et al*., 2010; Uday and Singh, 2013a, 2013b; Uday *et al*., 2015), also have important influences on the desiccation cracking behaviour. Despite significant research efforts on soil cracking over the past few decades, many questions remain unanswered.

Layer thickness is one of the most dominating factors for crack morphology due to its various effects on the soil desiccation cracking behaviour (Khatun *et al*., 2015). Crack pattern and spacing can be controlled by layer thickness found in pastes made of clay, sand and water (Colina and Roux, 2000). The average length and width of cracks as well as crack density increase when clay layer thicknesses increase (Guo *et al*., 2018; Tang *et al*., 2008). Furthermore, layer thickness influences cracking water content (defined as the water content at which cracks first appear), with thicker layers having higher cracking water contents and vice versa (Nahlawi and Kodikara, 2006; Tang *et al*., 2011b; Tollenaar *et al*., 2017). On the other hand, critical cracking thickness, defined as the minimum thickness of clay layers above which cracks will form, has been considered by researchers as a means of preventing cracking (Costa *et al*., 2018; Khatun *et al*., 2015; Singh and Tirumkudulu, 2007; Tang *et al*., 2011c; Xia and Hutchinson, 2000). However, the initial water content, which influences soil particle arrangement during drying and consequently affects the initiation and formation of desiccation cracking in clay layers (Tang *et al*., 2010, 2011a), has not been considered in these studies. Therefore, it is important to develop a better understanding of the way that clay layer thickness combined with the initial water content influences cracking patterns and evolution.

In this study, the authors investigated the desiccation cracks (formation and prevention) in thin bentonite clay layers of varying thicknesses with a wide range of initial water contents. The critical crack phase boundary distinguishing cracked and non-cracked samples was observed in a constructed phase diagram, which is controlled by both clay layer thickness and initial clay-water content. This study also estimated the cracking water contents for the cracked samples. Furthermore, detailed morphological characteristics of cracks were presented using different image analysis techniques and statistical analyses. To achieve these goals, a comprehensive series of experiments and analyses was performed, which are discussed in the following sections.

Material and methods

Material properties

Sodium bentonite was used in this study. Bentonite is a geological term of soil materials that has high-swelling minerals called montmorillonite. The general chemical formula of bentonite is $Na_{0.033}[Al_{1.67}Mg_{0.33}]Si_4O_{10}[OH]_2$. Bentonite from the soil mechanics laboratory stock (ActiveGel 150 bentonite, activated sodium bentonite with high montmorillonite and low grit content) was used for the experiments. This bentonite is commercially available and originally found in Queensland, Australia. The properties of the bentonite used in this study are shown in Table 1.

Experimental methods

At first, bentonite was oven-dried and water was added to bentonite at a solid:liquid mass ratio between 1:12 and 1:22 to obtain slurries with initial water contents of 1200–2200%. A stirring rod and a lab mixer were used for making a homogeneous mixture. After preparing the slurries, the containers were sealed with aluminium foil to avoid water evaporation and kept in a cupboard to soak for 2–3 days. These uniform slurries were then placed on Petri dishes with various thicknesses for the tests. Unless stated otherwise, all thicknesses mentioned in the paper are final thicknesses – that is, measured at the end of drying. Final thicknesses were controlled through the initial amount of clay in the slurry. The thickest sample was 0.21 mm deep, synthesised with 6 g of clay, followed by 0.18 mm with 5 g of clay and so on, with each reduction of 1 g of clay yielding around a 0.03 mm reduction in thickness. The smallest sample was 0.09 mm deep, obtained from 2 g of clay. The final thickness was found to be independent of the initial water content of the samples, for the range of thicknesses and water content considered here. Special care was taken to make the surfaces of the samples as uniform as possible before dehydration started. The tests were continued until the samples are fully dried (details about drying are in the section headed 'Drying curves and crack formation'). Drying periods depend on the

Table 1. Typical properties of the bentonite used in this experiment (Shannon *et al*., 2010)

Property	Value
Swelling volume: ml/2 g	35
Bulk density: kg/m^3	900
Liquid limit: %	550.0
Plastic limit:%	36.0
Natural water content: %	8–15
Cation-exchange capacity: mE/100 g	75
Specific gravity	2.69

thickness and initial water content (as shown in Figure 4). Thicker samples, and those with a higher initial water content, took longer to desiccate (compared with thinner and initially drier samples, respectively).

The dimensions of glass Petri dishes were 140 mm (diameter) × 20 mm (height) × 2 mm (thickness). The experiments were conducted using a hotplate as temperature source (30 ± 2°C on the top surface of samples) to desiccate the samples. Desiccation takes place due to the evaporation from only the upper surface of the samples. Since bentonite slurries desiccate on solid Petri dishes, only lateral and vertical shrinkage occur. The difference in temperature between the hotplate and the surface of the samples was found to be no more than 3°C.

A digital liquid-crystal display (LCD) temperature gun (non-contact LCD laser infrared digital temperature gun; accuracy: ±1.5°C; resolution: ±1°C) was used to measure the surface temperature at multiple positions – for example, in the centre and near the edge of the sample – at different times throughout the experiment. The samples together with the hotplate were mounted on the top of the electronic balance to record the weight loss due to evaporation as shown in Figure 1. The weight was recorded at intervals of 60 s. In addition, in order to capture the images of crack patterns, a digital camera (Nikon D750) was installed over the top of the samples (at around 500 mm distance). Colour images (resolution of 42.6 µm/pixel) were recorded from the surface of the samples at 60 s intervals. At least three repetitions were conducted for each sample (with a given thickness and initial water content), and the morphological characteristics of the final crack patterns were analysed. The thicknesses of the dried samples were measured by using an LCD gauge micrometer digital vernier calliper (Mitutoyo; accuracy: ±0.01 mm; resolution: ±0.01 mm). In addition, at the end of the tests, some dried samples were scanned using scanning electron microscopy (SEM) to observe the particle volume fraction across the layers (details are in the section headed 'Scanning electron microscopy'). The schematic diagram of the experimental set-up is shown in Figure 1.

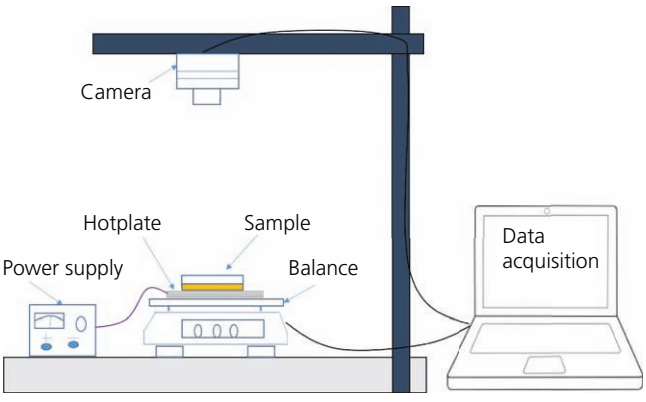

Figure 1. Schematic drawing of the experimental set-up

To investigate the water retention properties of specimens during dying, the gravimetric water content, w (%), was calculated as

$$w(\%) = \frac{w_w}{w_s} \times 100 \quad (1)$$

where w_w (g) is the mass of water in the sample and w_s (g) is the mass of the solid (clay) content.

Phase boundary detection

A phase diagram was constructed and tested in the laboratory. In the phase diagram, a phase boundary that distinguishes the cracked and non-cracked samples was identified. A theoretical model was developed to predict this phase boundary by modifying the model for critical cracking thickness originally proposed by Goehring *et al*. (2015). Using Griffith's fracture criterion, Goehring *et al*. (2015) calculated the critical cracking thickness of clay below which cracks will not occur under desiccation.

The model was simplified in terms of the fracture toughness and shear strength of clay materials. Both the fracture toughness and shear strength were then expressed as a function of water content following empirical relationships taken from the literature. However, the critical thickness needs to be related to initial water contents in order to predict the phase boundary. For this purpose, the water content was converted to the initial water content by assuming a linear distribution of clay particle volume fraction over the layer thickness. Thus, the model developed in this study could predict the phase boundary (between crack formation and prevention) for combined effects of layer thickness and initial water content on desiccation cracks. Details of the model derivation are provided in the section headed 'Crack prevention'.

Scanning electron microscopy

At the end of the desiccation test, dried films were chosen from different positions across the sample and investigated using SEM (Zeiss Sigma VP HD) to observe the clay particle distribution throughout the layer. SEM was conducted across the layer (the cross-section) as well as on both the top and bottom surfaces of the layer. The sample was first cut into small pieces by using a small knife. For the top/bottom surface observations, the sample was placed on a SEM stub with a carbon adhesive tape. For the cross-sectional observation, the sample was kept in the slotted stub to have the surface exposed for scanning. The extra clay layers were removed using a fan. The sample was grounded on the stub using silver painting to avoid the charging effect. Afterwards, the sample was coated by gold sputtering (Emitech K550X) using 25 mA for 2 min in order to obtain a 15 nm thick gold layer. The sample was then taken for SEM imaging, where the sample was scanned in the secondary electron mode for surface morphology. All SEM images were taken at an accelerating voltage of 5 kV and a working distance of approximately 5 mm with an aperture of 60 µm.

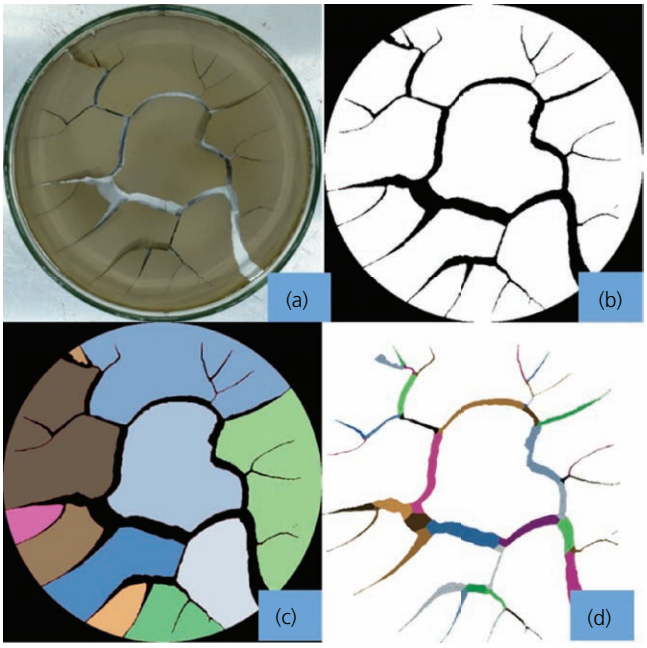

Figure 2. Image-processing techniques used in this study: (a) original image; (b) binarised image after noise removal and crack restoration; (c) cell details; (d) crack quantification

Image processing

A series of image analysis techniques was applied to analyse the morphology of crack patterns. The procedure of image processing is shown in Figure 2. The original images were preprocessed using standard algorithms of Matlab (Figures 2(a) and 2(b)). At first, cracks at edges were ignored so as to remove boundary effects (Costa *et al*., 2008). Light reflection was then cleared using Lab thresholding before converting the images to greyscale. Afterwards, different morphological techniques, such as noise removal, crack smoothing and crack restoration, were used to process the final binary images (Shokri and Or, 2013). Binary images were then used in the Pore and Crack Analysis System (Pcas) software to quantify the cell (uncracked area surrounded by cracks) and cracks (Figures 2(c) and 2(d)). Details of the Pcas software program can be found in the paper by Liu *et al*. (2013). In summary, the Pcas software program gives the total crack area, individual crack areas, lengths, widths and numbers. These results were used for statistical analysis to quantify the crack patterns later in the section headed 'Results and discussion'.

Statistical analysis

To understand better the geometrical characteristics of crack patterns, the following quantitative parameters were calculated: (*a*) crack density, which is the ratio of the total crack area to the total surface area (Lu *et al*., 2015); (*b*) total crack length, which is the sum of all individual crack lengths (Lakshmikantha *et al*., 2009); (*c*) average

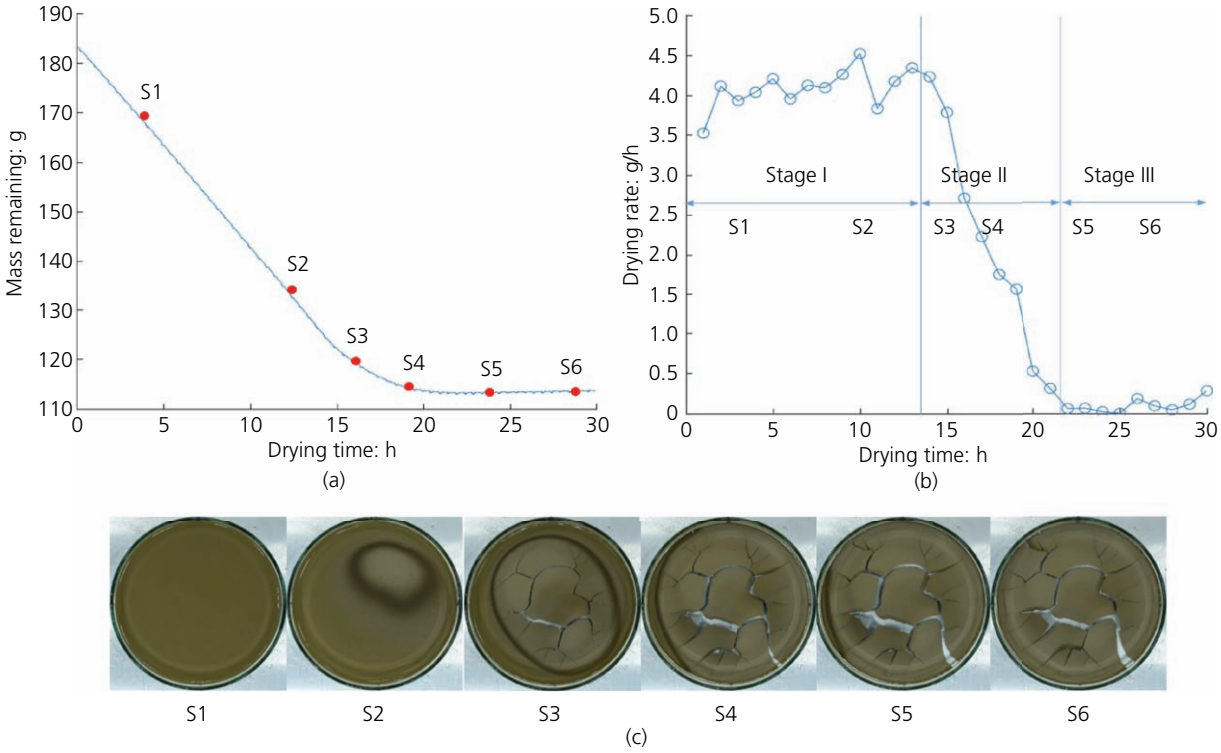

Figure 3. Crack development stages with drying time for a sample thickness of 0.18 mm and an initial water content of 1400%: (a) changes in mass over the drying period; (b) drying rate over the drying period; (c) crack evolution of desiccating bentonite at varying intervals. Here, S1 to S6 refer to different steps during three stages

crack length, defined as the mean of all individual crack lengths; (*d*) average crack width, the mean of all individual crack widths; and (*e*) probability density of crack lengths and widths. Since the distributions of crack length and width follow a typical log-normal distribution (Hudson and Priest, 1979; Li *et al.*, 2011; McKay *et al.*, 1993), the maximum likelihood estimation (MLE) of log-normal distributions was used to estimate the fitting parameters of statistical models. The well-known probability density function (PDF) of a log-normal distribution is

$$f(x|\mu,\sigma^2) = \frac{1}{x\sqrt{2\pi\sigma^2}}\exp\left\{-\frac{[\ln(x)-\mu]^2}{2\sigma^2}\right\} \quad (2)$$

where x ($x > 0$) is the observed data and μ and σ^2 are the logarithmic mean and variance of the distribution, respectively. The likelihood function of the log-normal distribution is

$$L(\mu,\sigma^2|x) = \prod_{i=1}^{n}\frac{1}{x_i\sqrt{2\pi\sigma^2}}\exp\left\{-\frac{[\ln(x_i)-\mu]^2}{2\sigma^2}\right\} \quad (3)$$

The likelihood function needs to be optimised with respect to parameters μ and σ^2, where $-\infty < \mu < \infty$ and $\sigma^2 > 0$. Thus, setting the derivative to zero, the MLEs of μ and σ^2 are

$$\acute{\mu} = \frac{\sum_{i=1}^{n}\ln x_i}{n} \quad (4)$$

and

$$\acute{\sigma}^2 = \frac{\sum_{i=1}^{n}(\ln x_i - \acute{\mu})^2}{n} \quad (5)$$

Results and discussion

Drying curves and crack formation

The desiccation progress of samples and drying curves, which indicate changes in the water content with time and the corresponding crack development, are shown in Figure 3. On drying, the water content (i.e. mass remaining, defined as a mass that remains after deducting the mass lost due to evaporation from total mass of the sample) decreased rapidly at the beginning of the tests. It then reduced gradually before it flattened to nil and the water content reached a steady condition (Figures 3(a) and 4). This condition indicates that the hydraulic steady state has been reached, which was found to correspond to less than 10% in water content as seen in Figure 4, and drying is finished. Three stages can be discerned when examining the drying rates (the slope of the drying curve is defined as a drying rate) in Figure 3(b): evaporation period (stage I), sharp decreasing transition period (stage II) and low-rate evaporation period (stage III). The water content decreases linearly during stage I, and the drying rate is almost the same and higher (about 4.0 g/h) than at any other stage. In stage II, the water content continues to decline but the drying rate falls sharply. Finally, evaporation enters a stable stage (stage III) and almost ceases. The majority of cracks are generated at the second stage (S3 and S4 in Figure 3(c)). There are no major changes in crack patterns in the last stage (S5 and S6 in Figure 3(c)) compared with the second stage (S3 and S4 in Figure 3(c)). In the last stage, existing cracks widen slightly and thin cracks appear. This is illustrated for a typical example (layer thickness is 0.18 mm and initial water content is 1400%) that is true for all other samples. Similar results were reported by Shokri and Sahimi (2012) and Zhang *et al.* (2017).

It is generally proposed that cracks develop due to an increase in capillary suction and tensile stress in the clay layer (Yesiller *et al.*, 2000). When the water content decreases during drying, the contact angle of the capillary meniscus increases, and thus, capillary suction as well as effective stress increases. As a result,

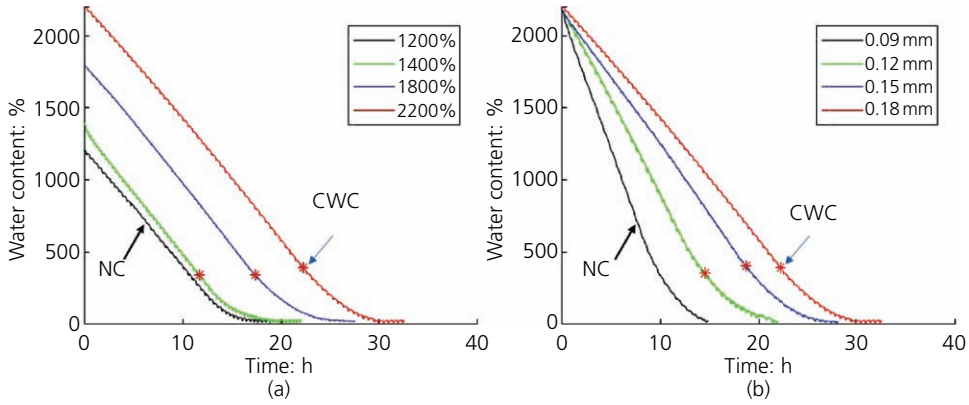

Figure 4. Drying curves and critical water content with drying time: (a) different water contents for the same thickness (0.18 mm); (b) different layer thicknesses for the same initial water content (2200%). NC refers to uncracked samples, and CWC refers to the critical water content for cracked samples (stars indicate points at which cracking first occurs)

clay layers consolidate and shrinkage occurs. Once the developed tensile stress due to shrinkage exceeds the tensile strength of the clay layer, cracks initiate on the surface (Tang *et al.*, 2011a). In this experiment, as bentonite slurry dehydration proceeds, a large volume change (i.e. shrinkage) occurs due to the water loss. This volume change is accommodated by the formation of cracks.

Figure 4 shows drying curves for various initial water contents and layer thicknesses. Under higher water contents and for thicker layers, cracks take longer to initiate and finish desiccation. The water content at which a crack first occurs is called the critical water content (Corte and Higashi, 1964; Lakshmikantha *et al.*, 2018; Nahlawi and Kodikara, 2006; Tang *et al.*, 2011a). Figure 4 shows that the critical water content was not influenced much by the changes in both layer thicknesses and initial water contents, at least not for the ranges considered here, with the critical water content always between 335 and 390%. This finding is not consistent with those of Corte and Higashi (1964), who reported that the critical water content increases when the sample thickness increases (between 3.5 and 33.5 mm). However, the results of Nahlawi and Kodikara (2006) and Sima *et al.* (2014) showed that small differences in layer thicknesses (6–10 mm) alone may not change the critical water content. The water content gradient along the vertical direction may be one possible reason behind this fact (Tang *et al.*, 2010). According to the study by Peron *et al.* (2009b), a higher water content gradient along the vertical direction causes greater tensile stress. This means that cracks occur at higher water contents in thicker samples. In the case of the present study, samples are considerably thin, so the difference in water content across the thickness is small and the observed cracking water content seems to be quite stable compared with different samples (Figure 4). Rodríguez *et al.* (2007) also reported that critical water contents may not change noticeably in very thin layers. Here, the critical water content refers only to the transient stage of the initial crack for individual samples during desiccation.

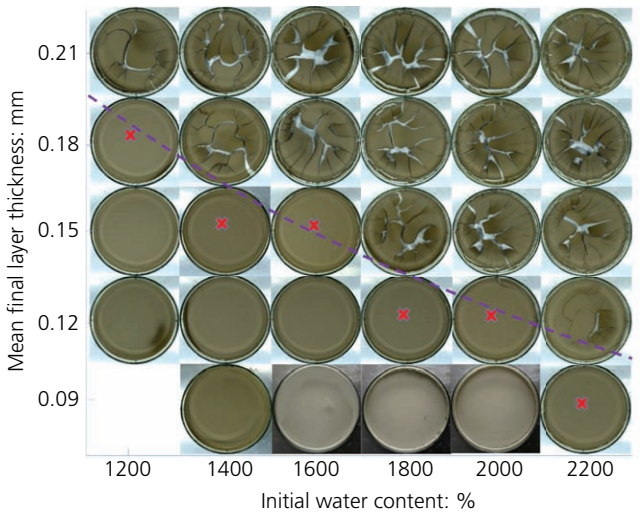

Figure 5. Phase diagram and crack patterns of thin bentonite clay layers. The sample in the blank (bottom left of the figure) was not tested assuming that this one would be a non-cracked sample. Crosses represent the critical thickness, and the average dashed line drawn based on the critical thickness is defined as the phase boundary

Crack prevention

As shown in Figures 3 and 4, crack evolution and morphology depend on the initial water contents and layer thicknesses. Thus, in order to investigate the cracking behaviour, a phase diagram was constructed and tested in this study (Figure 5). Figure 5 shows that in several cases, no cracks appear even after complete drying; it reveals, furthermore, that there is a critical thickness above which cracking occurs (Khatun *et al.*, 2015; Santanach *et al.*, 2007). The figure also shows that the critical thickness (i.e. crack-free layer as crack prevention) does not depend only on clay layer thickness but also on the initial water content. Other works (Ávila *et al.*, 2005; Tollenaar *et al.*, 2017) also reported that the initial water content has influence over the formation and morphology of the desiccation cracks. Based on the critical thicknesses (crosses in Figure 5), an average line is drawn and defined as a crack phase boundary, which distinguishes between cracked and non-cracked samples.

In order to obtain the final thickness of the phase diagram, some broken layers of the desiccated samples were taken and measured using a digital slide calliper. Thicknesses vary from around 0.09 to about 0.21 mm (Table 2). The mean thicknesses of the final layers are shown in Figure 5 against the initial water contents.

As defined in Figure 5, the phase boundary reveals a border between crack formation and prevention in the phase diagram. When the layer thickness exceeds the critical thickness value,

Table 2. Mean values of the measured final thickness of the dried clay film for different initial water contents (in %)

Number	Final thickness: mm						
	1200%	1400%	1600%	1800%	2000%	2200%	Mean
1	0.21(0.01)	0.21(0.02)	0.20(0.01)	0.22(0.01)	0.20(0.03)	0.21(0.04)	0.21
2	0.18(0.01)	0.18(0.01)	0.18(0.01)	0.18(0.01)	0.18(0.01)	0.17(0.01)	0.18
3	0.14(0.01)	0.14(0.01)	0.14(0.01)	0.14(0.01)	0.16(0.01)	0.15(0.02)	0.15
4	0.11(±0.01)	0.12(±0.01)	0.13(±0.01)	0.12(0.01)	0.13(0.02)	0.12(0.01)	0.12
5	—	0.09(0.01)	0.09(0.01)	0.09(0.01)	0.09(0.01)	0.09(0.0)	0.09

Standard deviations around the mean of measurements from three repetitions for each test are shown in parentheses, and the values are in millimetres

crack occurs in any materials (Santanach *et al*., 2007; Singh and Tirumkudulu, 2007). Thus, the critical thickness can be used to determine the phase boundary separating cracked and non-cracked zones in the constructed phase diagram. Griffith's fracture criterion, based on the change in free energy caused by the crack, takes into account internal strain-energy release and surface energy as a result of crack formation. Hence, the critical cracking thickness, h_c (m), is given by (Goehring *et al*., 2015)

$$h_c = \frac{\Omega E' G_{Ic}}{\sigma_{max}^2} \quad (6)$$

where Ω is a constant (i.e. 0.8 for soils; see the book chapter by Goehring *et al*. (2015) for details); E_1' (kPa) is the plane strain elastic modulus; G_{IC} (kN/m) is the critical strain-energy release rate; and σ_{max} (kPa) is the maximum stress during drying before cracks appear. E_1', the plane strain elastic modulus, is defined as (Goehring *et al*., 2015)

$$E' = \frac{E}{1 - \nu^2} \quad (7)$$

where E (kPa) is the Young's modulus of clay and ν is the Poisson's ratio of clay. G_{IC} (kN/m) is the critical strain-energy release rate and can be expressed by (Lakshmikantha *et al*., 2012)

$$G_{IC} = \frac{K_{IC}^2}{E} \quad (8)$$

where K_{IC} (kN/m$^{1.5}$) is the fracture toughness of clay slurry. Combining Equations 6–8, the critical cracking thickness can be written as

$$h_c = \frac{\Omega}{1 - \nu^2}\left(\frac{K_{IC}}{\sigma_{max}}\right)^2 \quad (9)$$

Using the well-known size-effect law, the maximum stress can be expressed in terms of the tensile strength (σ_t (kPa)) as (Bažant, 1984; Lakshmikantha *et al*., 2012)

$$\sigma_{max} = \frac{\lambda \sigma_t}{\sqrt{(1 + d/\lambda_0 d_0)}} \quad (10)$$

where d (mm) is the specimen characteristic dimension (here, diameter of the sample); d_0 (mm) is the reference dimension (e.g. maximum particle size); λ and λ_0 are two parameters that can be determined from regression analysis ($\lambda \cong 1.48$ and $\lambda_0 \cong 479.5$; see the paper by Lakshmikantha *et al*. (2012) for details). Substituting Equation 10 into Equation 9, the critical cracking thickness becomes

$$h_c = \frac{\Omega(1 + d/\lambda_0 d_0)}{(1 - \nu^2)\lambda^2}\left(\frac{K_{IC}}{\sigma_t}\right)^2 \quad (11)$$

Since Ω, ν, d, d_0, λ and λ_0 are material-dependent constants, Equation 11 can be simplified and written as

$$h_c = C\left(\frac{K_{IC}}{\sigma_t}\right)^2 \quad (12)$$

where C can be defined as combined material constant and $C = \Omega(1 + d/\lambda_0 d_0)/(1 - \nu^2)\lambda^2)$, where Ω is the material constant for critical cracking thickness. Equation 12 is an expression of the critical thickness of soil layer below which cracks do not occur. Experimental evidence shows that the term $(K_{IC}/\sigma_t)^2$ in Equation 12 decreases when the material becomes brittle (Costa *et al*., 2018), and some studies have developed a relationship between K_{IC} and σ_t (Xu *et al*. 2018).

Fracture toughness can be obtained as a function of the water content (w (%)) through the following empirical relationship (Costa, 2009):

$$K_{IC} = a_1 \exp(-b_1 w) \quad (13)$$

where a_1 (kN/m$^{1.5}$) and b_1 (/%) are fitting parameters (e.g. a_1 = 897.76 kN/m$^{1.5}$ and b_1 = 0.1076/% for Werribee Clay; details in Table 3). Tensile strength has also been expressed as a function of water content (Costa, 2009; Stirling *et al*., 2015; Trabelsi *et al*., 2012) as

Table 3. Values of parameters a (= a_1/a_2) and b (= $b_1 - b_2$) for different clays

a_1: kN/m$^{1.5}$	a_2: kPa	b_1: /%	b_2: /%	Soil	Reference
897.76		0.1076		Werribee Clay	Costa (2009)
1018.9		0.1148		Merri Creek Clay	Costa (2009)
272.25		0.204		Silty clay	Nichols and Grismer (1997)
116.18		0.112		Silty clay (local)	Wang *et al*. (2007)
	148.97		0.039	Werribee Clay	Amarasiri *et al*. (2011)
	148.65		0.066	Beja Clay	Trabelsi *et al*. (2012)
	305.05		0.111	Silty clay (local)	Wang *et al*. (2007)
	144.937		0.1252	Loess (clay)	Wang *et al*. (2001)

14. $$\sigma_t = a_2 \exp(-b_2 w)$$

where a_2 (kPa) and b_2 (/%) are fitting parameters (e.g. a_2 = 148.97 kPa and b_2 = 0.039/% for Werribee Clay; details in Table 3).

Substituting Equations 13 and 14 into Equation 12, the critical cracking thickness becomes

15. $$h_c = C[a \exp(-bw)]^2$$

where $a = a_1/a_2$ ($m^{0.5}$) and $b = b_1 - b_2 (b_1 > b_2)$ (/%). The values of the parameters depend on the types of clay as well the experimental methods used in the laboratory (Xu *et al.*, 2018). As shown in Table 3, although there are many variations, values of a and b could have a range of 0.4–6.0 $m^{0.5}$ and 0.001–0.0686/%, respectively (considering the Werribee Clay and local silty clay). For the sake of simplicity of the model, the value of a has been taken as constant (0.40). The parameter b will be considered as a fitting parameter to predict the experimental results. Therefore, Equation 15 can be written further as

16. $$h_c = C_f[\exp(-bw)]^2$$

where C_f can be defined as material constant for fracture and $C_f = Ca^2$ (m). In this study, it is 2.096 m, with calculation details presented in the Appendix (which also includes Figure 13).

In Equation 16, water content (w) is the current water content of the clay slurry. In order to predict the phase boundary found in the phase diagram (Figure 5), the current water content needs to be related to the initial water content. This relationship could be established by the clay particle volume fraction distribution within the layer thickness.

During hydration, water evaporates from the top surface, and thus, clay particles come closer and closer. As a result, the mixture becomes denser at the top surface of the layer compared with the bottom one. Thus, the volume fraction of clay particles is likely to be a depth-dependent parameter during dehydration of the samples. In light of this concept, the following assumptions are made in order to generate a reasonably simple relationship between clay volume fraction and initial water content:

- The particle volume fraction of clay (ϕ) is linearly distributed across the depth of the sample during dehydration so that ϕ is higher at the top compared with the bottom (Figure 6).
- The slope k of the ϕ distribution is equal to α times the initial particle volume fraction (ϕ_i) divided by the final film thickness (h) of the layer, with the particle volume fraction given by (Figure 6)

17. $$\phi(h) = \phi_0 \pm kh \quad \text{and} \quad k = \alpha \frac{\phi_i}{h}$$

where ϕ_0 is the average volume fraction and $\alpha (0 < \alpha \leq 2)$ is a parameter that depends on both material properties and environmental conditions (temperature, humidity, etc.)

- Given that in experiments reported in this paper, the layer is considerably thin and the temperature difference between the top and bottom surfaces is small, the temperature gradient across the thickness of the sample is negligible.

SEM images (Figure 7) of the dried clay layer show that the particles are more homogenised at the top surface compared with the bottom one. This homogenisation of the clay particles can be regarded as a reflection of the particle volume fraction (density) and is broadly consistent with the assumption of linear variation of the particle volume fraction of clay.

Now, the particle volume fraction of clay is

18. $$\phi = \frac{1/\rho_p}{1/\rho_p + 0.01w/\rho_w} = \frac{1}{1 + 0.01 G_s w}$$

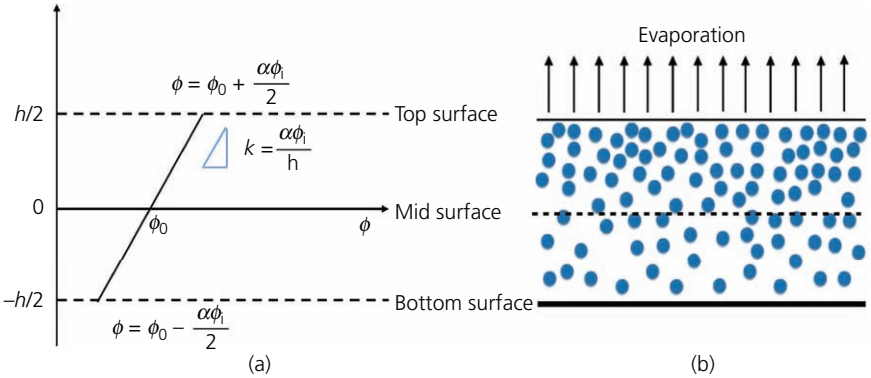

Figure 6. Distribution of clay particle volume fraction (ϕ) within the thickness (h) of layer: (a) linear distribution of ϕ showing the variations between the top and bottom surfaces; (b) simple representation of clay particles on evaporation (desiccation)

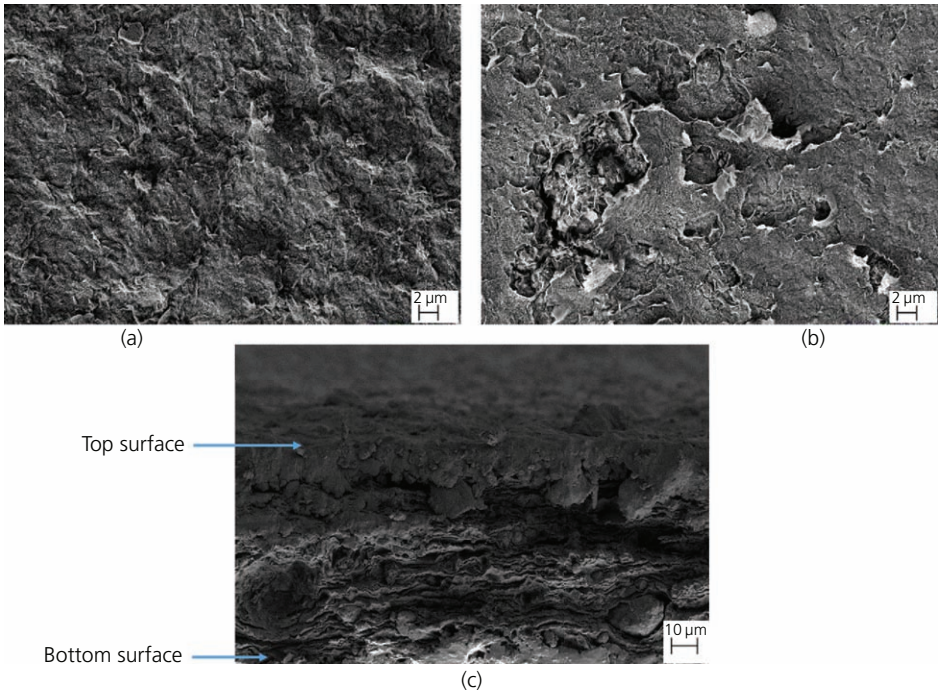

Figure 7. SEM images of the dried clay layer: (a) top surface; (b) bottom surface; (c) along the side (cross-section) (images refer to the sample of Figure 5 where the layer thickness is 0.18 and the initial water content is 1800%)

where ρ_p (kg/m^3) is the clay particle density, ρ_w (kg/m^3) is the density of water and G_s is the specific gravity of clay. Thus, the water content (w(%)) in terms of clay particle volume fraction can be written as

$$w = \frac{1-\phi}{0.01 G_s \phi} \quad (19)$$

Using the assumptions detailed above and Equations 17–19, the relationship between the particle volume fraction of clay (at the top surface) and the corresponding water content becomes

$$w = \frac{1-(\phi_0 + \alpha\phi_i/2)}{0.01 G_s(\phi_0 + \alpha\phi_i/2)} \quad (20)$$

where ϕ_0(= $1/(1 + 0.01\, G_s w_0)$) is the critical volume fraction of clay and ϕ_i(= $1/((1 + 0.01\, G_s w_i)$) is the initial volume fraction of clay, where w_0 (%) and w_i (%) are the critical (cracking) water content and initial water content, respectively. Variation of the water content with initial water contents is shown in the Appendix. Thus, the final expression for the critical cracking thickness can be written as

$$h_c = C_f \left[\exp\left\{-b\left[\frac{1-(\phi_0 + \alpha\phi_i/2)}{0.01 G_s(\phi_0 + \alpha\phi_i/2)}\right]\right\}\right]^2 \quad (21)$$

The model given by Equation 12 has two fitting parameters: α and b. The values of model parameters used to predict the phase boundary for the experiments reported earlier are shown in Table 4. It is found that the best-fit value for b is 0.0145, which falls well within the range of 0.001–0.0686/%, reported in the literature for a range of different clays (Amarasiri *et al.*, 2011; Costa, 2009; Wang *et al.*, 2007).

Prediction of the phase boundary yielded by Equation 21 is shown in Figure 8, as well as its sensitivity to the fitting parameters. The model predictions show good agreement with experimental data.

Crack morphology

Tables 5 and 6 show changes in the values of descriptive crack parameters with the initial water content and layer thickness. Three water contents (1400, 1800 and 2200%) and three clay layer thicknesses (0.15, 0.18 and 0.22 mm) are considered here. It can be seen that crack properties, such as crack density, total crack length and average crack length and width, increase with increasing initial water content and layer thickness. These results

Table 4. Values of model parameters

Parameter	Value	Unit	Source
v	0.26	—	Wang *et al.* (2001)
d	140	mm	This study (plate size)
d_0	9	μm	This study (clay particle size)
w_0	341.7	%	This study (critical water content)
α	0.71	—	Fitting values
b	0.0145	/%	Fitting values

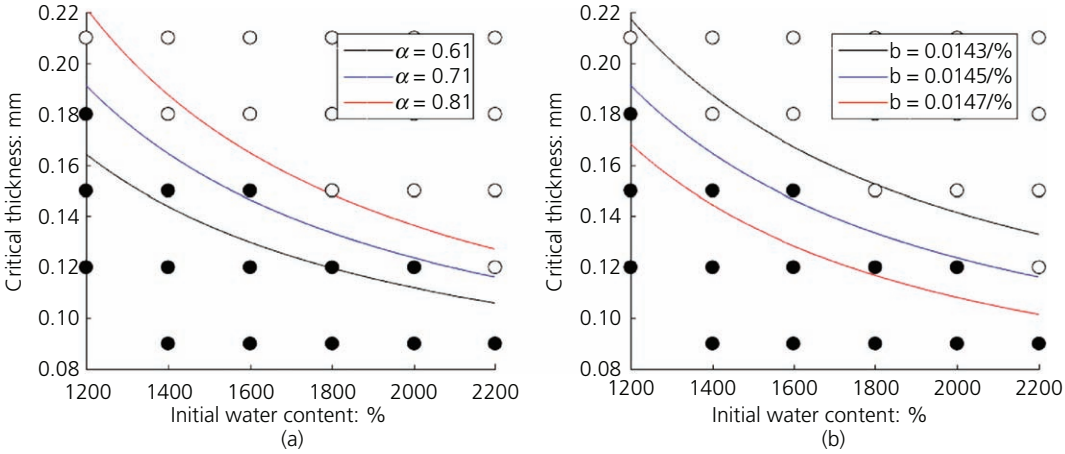

Figure 8. Phase boundary comparisons between experimental data and model predictions: (a) sensitivity to α with b = 0.0145/%; (b) sensitivity to b with α = 0.71. Here, filled circles indicate uncracked samples and empty circles represent cracked samples

Table 5. Effect of initial moisture content (in %) on crack morphology (layer thickness is 0.18 mm)

Number	Crack property	1400%	1800%	2200%
1	Crack density: mm^2/mm^2	0.10(0.02)	0.14(0.04)	0.13(0.04)
2	Total crack length: mm	687.55(50.73)	747.81(49.0)	818.47(94.75)
3	Average crack length: mm	18.17(2.11)	21.39(4.48)	21.96(2.19)
4	Average crack width: mm	1.40(0.28)	2.44(0.62)	2.03(0.52)
5	Crack number	38(3)	36 (5)	38(7)

Values in the parentheses are the corresponding standard deviations

Table 6. Effects of layer thickness (in mm) on crack morphology (initial water content is 2200%)

Number	Crack property	0.15 mm	0.18 mm	0.22 mm
1	Crack density: mm^2/mm^2	0.12(0.01)	0.13(0.04)	0.13(0.01)
2	Total crack length: mm	753.56(170.49)	818.47(94.75)	809.75(277.75)
3	Average crack length: mm	18.50(0.77)	21.96(2.189)	20.31(0.92)
4	Average crack width: mm	1.97(0.19)	2.03(0.52)	2.34(1.04)
5	Crack number	41(11)	38(7)	40(15)

Values in parentheses are the corresponding standard deviations

are consistent with the findings of Tang *et al*. (2008). However, the initial water content and layer thickness do not appear to have any influence on crack numbers. For example, crack numbers fall within 38–41 on average.

Crack density is more sensitive to changes in the initial water content than changes in thickness within the ranges considered here. Crack density increases from 0.10 to more than 0.13 (mm^2/mm^2) when the initial water content rises from 1400 to 2200% (Table 5). On the other hand, no significant change in crack density (i.e. 0.12–0.13 mm^2/mm^2) is observed when the layer thickness increases from 0.15 to 0.22 mm (Table 6). The total crack length is higher in thicker layers and, in larger water contents, falls between 687.5 and 818.5 mm (for w_i between 1400 and 2200%) and between 753.5 and 818.5 mm (for h between 0.15 and 0.22 mm). Average crack lengths and widths also increase with increments in water content and layer thickness, and average crack widths appear to be more sensitive than average crack lengths, indicating that increases in specimen thickness would increase the probability of forming longer and wider cracks.

Figures 9 and 10 show the probability distributions of crack lengths at different initial moisture contents and clay layer thicknesses. For distributions of crack lengths, four water contents and layer thicknesses are presented. The distributions of crack lengths show the log-normal distributions in all cases. As stated earlier (Equations 2–5), the MLEs of log-normal fits show that crack lengths fall mainly within 0–50 mm. The maximum frequencies were observed for 10–20 mm of crack lengths in all cases. If the layer thickness is small with a high initial water content, crack lengths can be much longer. This might be due to the more uniform suction profile, which allows the crack to continue rather than branch into new cracks (Costa *et al*., 2018). The mean value shows an increasing trend due

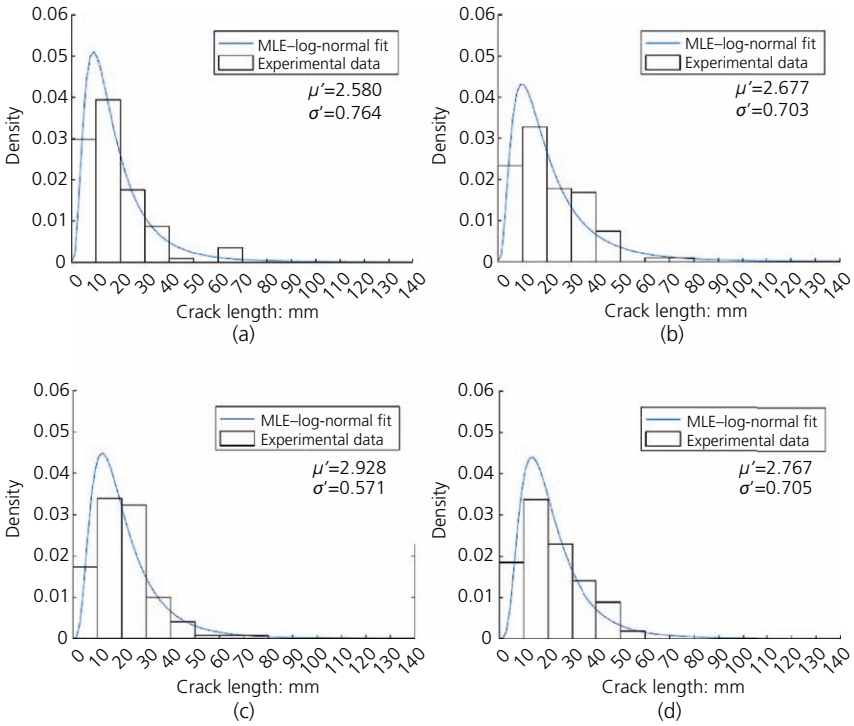

Figure 9. Crack length distributions for different water contents: (a) 1400%; (b) 1800%; (c) 2000%; (d) 2200%. The clay thickness for all cases is 0.18 mm

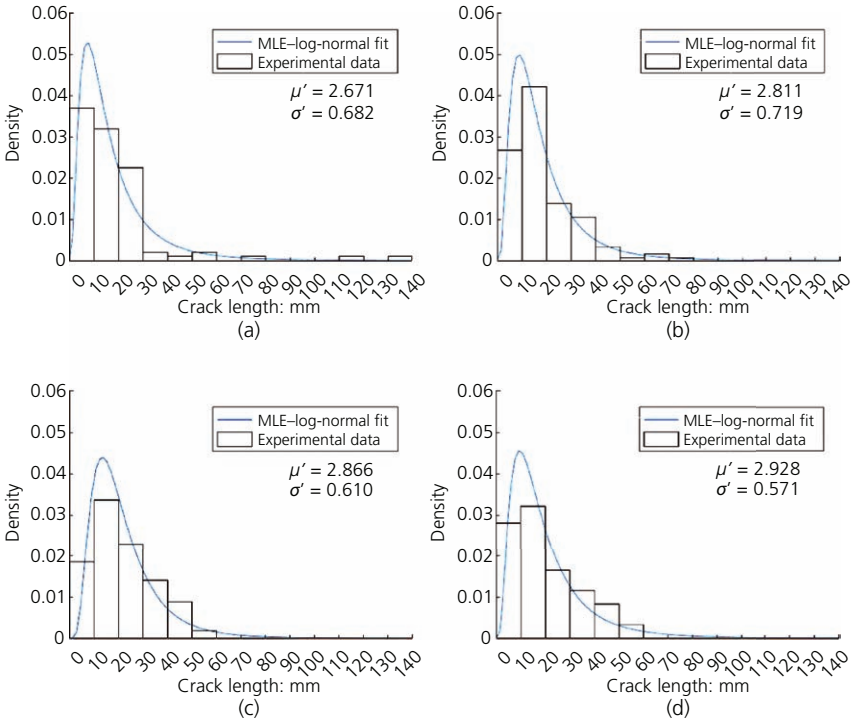

Figure 10. Crack length distributions for different layer thicknesses: (a) 0.12 mm; (b) 0.15 mm; (c) 0.18 mm; (d) 0.22 mm. The initial content for all cases is 2200%

to the increase in water content as well as in layer thickness. However, there are no clear trends in the standard deviations for variations in water content and layer thickness.

The PDFs of crack widths due to the effects of initial water contents and layer thicknesses are also presented in Figures 11 and 12. Similar to crack lengths, crack widths show log-normal distributions. The MLEs of log-normal fits match nicely with the experimental results. Most crack widths are in the range of 0–5 mm. Peak values are always observed within the interval 0–1 mm. As the initial water content or layer thickness increases, more wider cracks appear (Figures 11 and 12). Changes in water contents and layer thicknesses have little influence on both mean and standard deviation values for crack width.

By analysing the results shown in Tables 5 and 6 and Figures 9–12, it can be stated that crack properties, with the exception of crack numbers, are influenced by both the initial water content and layer thickness. Crack properties are influenced more by changes in water contents than changes in layer thicknesses, bearing in mind the limited thickness range considered here. The vertical suction profile could be one reason for this fact. When water evaporates at the surface of the sample during desiccation, water moves from the bottom to the surface as a result of capillary action creating a suction profile along the depth (Costa *et al*., 2008). For thinner layers, the suction gradient is smaller and the cracks are more likely extended to a full depth when initiated (Kodikara and Choi, 2006). Thus, thinner layers are less influenced by the suction profile. On the other hand, as a wet cohesive soil undergoes desiccation, soil particles become dense and come closer. When desiccation starts from the surface and moves downwards, the dehydrated surface shrinks. Adjustments preventing this shrinkage between top and bottom surfaces create more tensile stress (Tang *et al*., 2008), and thereby, the layer breaks and cracks occur. Thus, a higher initial water content (at least some ranges as found by Kassiff and Shalom (1971)) may cause more shrinkage, with the desiccation accommodating this volume change into cracks (Ávila *et al*., 2013).

Key findings

In this study, a comprehensive series of experiments was performed in order to capture desiccation and cracking behaviour under different conditions. The drying and cracking phases were tracked with photographic monitoring and weighing of samples, followed by SEM and image analyses, as well as statistical description of crack morphology. The authors have elicited the key features of the genesis of desiccation crack in bentonite clays, particularly as they are affected by the layer thickness and initial water content, and found that both these variables influence crack formation and prevention. Results presented in terms of phase diagrams revealed important information about the crack formation process in clays. The theoretical model developed here considers the initial water content and proceeds from an assumption of depth-dependent porosity distribution. The model was found to be quite efficient in capturing the development of desiccation cracks, in particular distinguishing

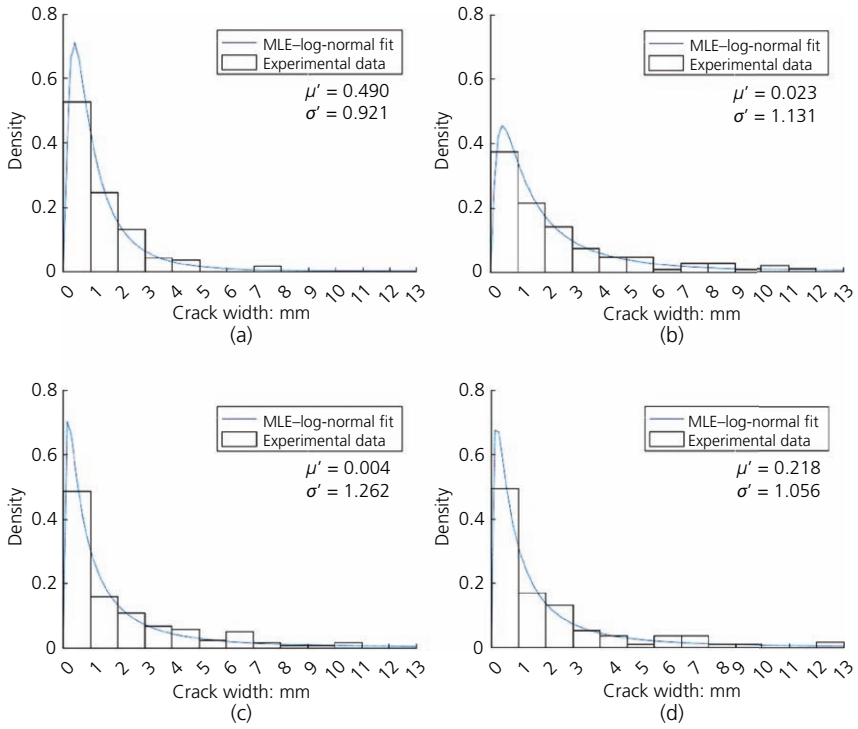

Figure 11. Crack width distributions for different water contents of (a) 1400, (b) 1800, (c) 2000 and (d) 2200% when the layer thickness is 0.18 mm

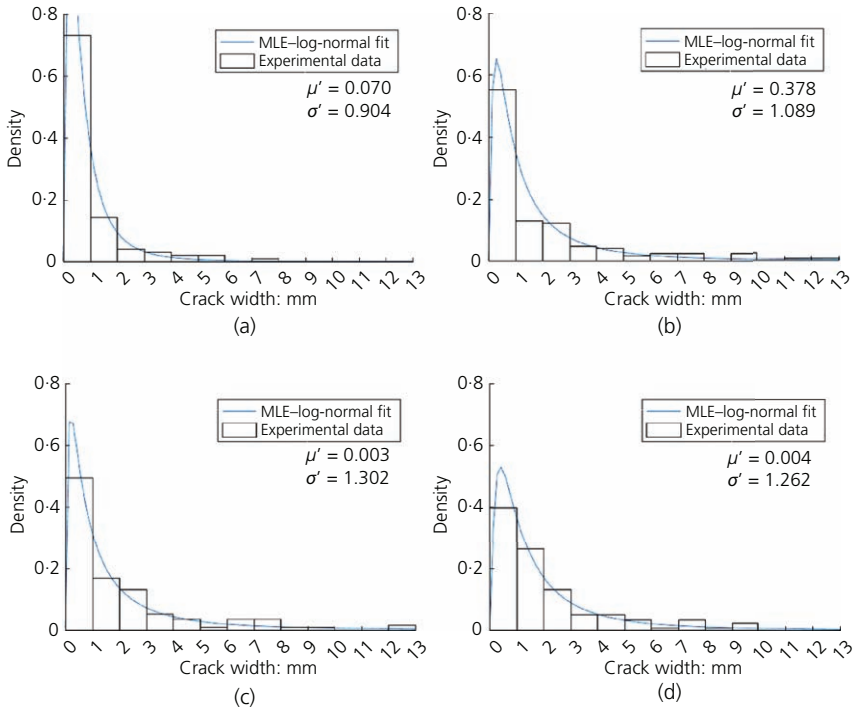

Figure 12. Crack width distributions for different layer thicknesses of (a) 0.12, (b) 0.15, (c) 018 and (d) 0.22 mm when the water content is 2200%

between cracked and non-cracked zones and predicting the crack phase boundary. Hence, the model proposed here can be used to explore the desiccation behaviour of other types of clay as well as the influence of variables other than those considered here (thickness and water content), including, among others, sample diameter, rate of evaporation and friction between clay and sample container material.

Conclusion

Desiccation cracks in thin bentonite clay layers were investigated for a wide range of initial water contents in this study. A phase diagram, which is controlled by bentonite layer thicknesses and initial clay-water contents, was constructed and tested in the laboratory. Based on the results, the following conclusions were made.

- The critical crack thickness plays an important role in the phase diagram and distinguishes between cracked and non-cracked samples. The critical crack thickness could be used as an indicator of cracking and to detect the phase boundary depending on the initial water content and layer thickness.
- Changes in the initial water content for thin bentonite layers do not significantly influence the cracking water content under the conditions explored in this paper.
- Crack properties such as crack density, total crack length, average crack length and crack width increase with increasing layer thicknesses and initial water contents.
- Changes in initial water contents have more effects on crack morphology than changes in layer thicknesses within the ranges of the present investigation.

Two lines of investigation can be pursued as extension of this research. The range of thicknesses of the clay layer, considered in this paper, is small. Hence, the applicability of Equation 21 within a wider range of thicknesses would be of interest. More generally, the behaviour of soils, in particular bentonite, in nature is more complex, in part because of the influence of factors such as temperature, loading conditions and chemistry of pore water. Therefore, the applicability to field conditions of the insights and equations developed here remains an open question.

Acknowledgements

This work was financially supported by the Australian Research Council (project DP170104192). The authors acknowledge Mr Ross Barker and Mr Todd Budrodeen for their very kind co-operation to set up the experiment and supply the materials. The authors also greatly acknowledge Dr James Baker, postdoctoral research associate, for his valuable comments to improve the manuscript.

Appendix

Calculation of C_f (m):

$$C_f = \frac{\Omega\ (1 + d/\lambda_0 d_0)}{(1 - \nu^2)\lambda^2} \times a^2$$

$$C_f = \frac{0.8 \times \left[1 + 0.140/\left(479.5 \times 9 \times 10^{-6}\right)\right]}{\left(1 - 0.26^2\right)1.48^2} \times 0.4^2$$

22. $$C_f = 13.099 \times 0.4^2 = 2.096 \text{ m}$$

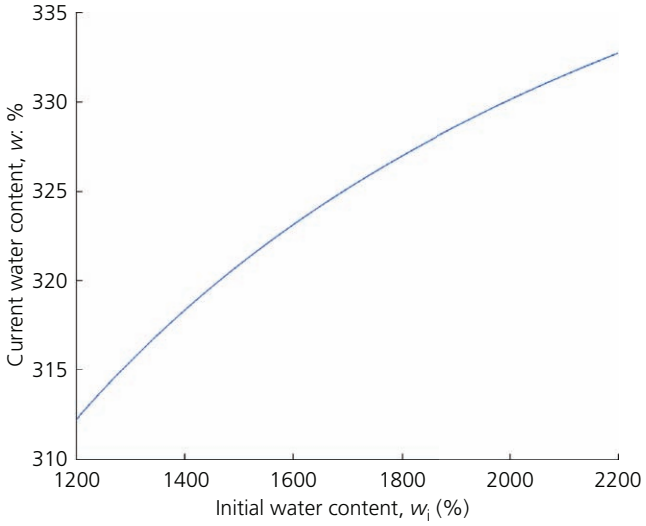

Figure 13. Current water content plotted against initial water content

The variations in the current water content with the initial water content is shown in Figure 13.

REFERENCES

Albrecht BA and Benson CH (2001) Effect of desiccation on compacted natural clays. *Journal of Geotechnical and Geoenvironmental Engineering* **127(1)**: 67–75, https://doi.org/10.1061/(asce)1090-0241(2001)127:1(67).

Amarasiri AL, Kodikara JK and Costa S (2011) Numerical modelling of desiccation cracking. *International Journal for Numerical and Analytical Methods in Geomechanics* **35(1)**: 82–96, https://doi.org/10.1061/(asce)1090-0241(2001)127:1(67).

Ávila G, Ledesma A and Lloret A (2005) Hydro-mechanical processes in soil desiccation problems. Application to Bogotá clay (Processus hydro-mécaniques de dessiccation des sols. Application a l'argile de Bogotá). In *Proceedings of the 16th International Conference on Soil Mechanics and Geotechnical Engineering 'Geotechnology in Harmony with the Global Environment'*. Millpress /IOS Press, Amsterdam, the Netherlands, vol. 4, pp. 2353–2356.

Ávila G, Ledesma A and Lloret A (2013) One-dimensional cracking model in clayey soils. *Proceedings of the 18th International Conference on Soil Mechanics and Geotechnical Engineering, Paris, France*, pp. 1077–1080.

Bažant ZP (1984) Size effect in blunt fracture: concrete, rock, metal. *Journal of Engineering Mechanics* **110(4)**: 518–535, https://doi.org/10.1061/(ASCE)0733-9399(1984)110:4(518).

Bronswijk JJB (1991) Relation between vertical soil movements and water-content changes in cracking clays. *Soil Science Society of America Journal* **55(5)**: 1220–1226.

Colina H and Roux S (2000) Experimental model of cracking induced by drying shrinkage. *European Physical Journal E* **1(2–3)**: 189–194.

Corte AE and Higashi A (1964) *Experimental Research on Desiccation Cracks in Soil*. US Cold Regions Research and Engineering Laboratory, Hanover, NH, USA.

Costa WDSM (2009) *Study of Desiccation Cracking and Fracture Properties of Clay Soils*. PhD thesis, Monash University, Melbourne, Australia.

Costa S, Kodikara J and Thusyanthan NI (2008) Modelling of desiccation crack development in clay soils. *Proceedings of the 12th International Conference of IACMAG, Goa, India*, pp. 1099–1107.

Costa S, Kodikara J and Shannon B (2013) Salient factors controlling desiccation cracking of clay in laboratory experiments. *Géotechnique* **63(1)**: 18–29, https://doi.org/10.1680/geot.9.P.105.

Costa S, Kodikara J, Barbour SL and Fredlund DG (2018) Theoretical analysis of desiccation crack spacing of a thin, long soil layer. *Acta Geotechnica* **13(1)**: 39–49.

da Silva WP, da Silva CMDP, da Silva LD and de Oliveira FVS (2013) Drying of clay slabs: experimental determination and prediction by two-dimensional diffusion models. *Ceramics International* **39(7)**: 7911–7919.

Daniel DE and Brown KW (1987) Landfill liners: how well do they work and what is their future? In *Land Disposal of Hazardous Waste: Engineering and Environmental Issues* (Gronow JR, Schofield AN and Jain RK (eds)). Ellis Horwood, Chichester, UK, pp. 235–244.

DeCarlo KF and Shokri N (2014) Effects of substrate on cracking patterns and dynamics in desiccating clay layers. *Water Resources Research* **50(4)**: 3039–3051.

El-Zein A (2016) Resilience and vulnerability to climate change: challenges of temporal and geographical scales for geotechnical engineering. *Australian Geomechanics Journal* **51(2)**: 65–78.

Goehring L, Nakahara A, Dutta T, Kitsunezaki S and Tarafdar S (2015) Fracture mechanics. In *Desiccation Cracks and Their Patterns: Formation and Modelling in Science and Nature*. Wiley-VCH, Weinheim, Germany, pp. 35–67.

Guo Y, Han C and Yu X (2018) Laboratory characterization and discrete element modeling of shrinkage and cracking in clay layer. *Canadian Geotechnical Journal* **55(5)**: 680–688.

Hudson JA and Priest SD (1979) Discontinuities and rock mass geometry. *International Journal of Rock Mechanics and Mining Sciences & Geomechanics Abstracts* **16(6)**: 339–362, https://doi.org/10.1016/0148-9062(79)90001-9.

Jayanthi PNV, Kuntikana G and Singh DN (2017) Stabilization of fine-grained soils against desiccation cracking using sustainable materials. *Advances in Civil Engineering Materials* **6(1)**: 36–67.

Kassiff G and Shalom AB (1971) Experimental relationship between swell pressure and suction. *Géotechnique* **21(3)**: 245–255.

Khatun T, Dutta T and Tarafdar S (2015) Topology of desiccation crack patterns in clay and invariance of crack interface area with thickness. *European Physical Journal E* **38(8)**: 83.

Kodikara JK and Choi X (2006) A simplified analytical model for desiccation cracking of clay layers in laboratory tests. In *Unsaturated Soils 2006* (Miller GA, Zapata CE, Houston SL and Fredlund DG (eds)). American Society of Civil Engineers, Reston, VA, USA, pp. 2558–2569.

Lakshmikantha MR, Prat PC and Ledesma A (2009) Image analysis for the quantification of a developing crack network on a drying soil. *Geotechnical Testing Journal* **32(6)**: 505–515.

Lakshmikantha MR, Prat PC and Ledesma A (2012) Experimental evidence of size effect in soil cracking. *Canadian Geotechnical Journal* **49(3)**: 264–284.

Lakshmikantha MR, Prat PC and Ledesma A (2018) Boundary effects in the desiccation of soil layers with controlled environmental conditions. *Geotechnical Testing Journal* **41(4)**: 675–697, https://doi.org/10.1520/GTJ20170018.

Lau JTK (1987) *Desiccation Cracking of Soils*. MSc thesis, University of Saskatchewan, Saskatoon, SK, Canada.

Leao S (2014) Mapping 100 years of Thornthwaite Moisture Index: impact of climate change in Victoria, Australia. *Geographical Research* **52(3)**: 309–327, https://doi.org/10.1111/1745-5871.12072.

Li X (2014) *Shrinkage Cracking of Soils and Cementitiously-stabilized Soils: Mechanisms and Modeling*. PhD thesis, Washington State University, Pullman, WA, USA.

Li JH and Zhang LM (2011) Study of desiccation crack initiation and development at ground surface. *Engineering Geology* **123(4)**: 347–358.

Li JH, Zhang LM, Wang Y and Fredlund DG (2009) Permeability tensor and representative elementary volume of saturated cracked soil. *Canadian Geotechnical Journal* **46(8)**: 928–942.

Li JH, Zhang LM and Li X (2011) Soil-water characteristic curve and permeability function for unsaturated cracked soil. *Canadian Geotechnical Journal* **48(7)**: 1010–1031.

Liu C, Tang CS, Shi B and Suo WB (2013) Automatic quantification of crack patterns by image processing. *Computers & Geosciences* **57**: 77–80.

Lu H, Li J, Wang W and Wang C (2015) Cracking and water seepage of Xiashu loess used as landfill cover under wetting–drying cycles. *Environmental Earth Sciences* **74(11)**: 7441–7450.

McKay L, Cherry JA and Gillham RW (1993) Field experiments in a fractured clay till: 1. Hydraulic conductivity and fracture aperture. *Water Resources Research* **29(4)**: 1149–1162.

Morris PH, Graham J and Williams DJ (1992) Cracking in drying soils. *Canadian Geotechnical Journal* **29(2)**: 263–277.

Nahlawi H and Kodikara JK (2006) Laboratory experiments on desiccation cracking of thin soil layers. *Geotechnical and Geological Engineering* **24(6)**: 1641–1664.

Nichols JR and Grismer ME (1997) Measurement of fracture mechanics parameters in 664 silty-clay soils. *Soil Science* **162(5)**: 309–322.

Peron H, Hueckel T, Laloui L and Hu LB (2009a) Fundamentals of desiccation cracking of fine-grained soils: experimental characterisation and mechanisms identification. *Canadian Geotechnical Journal* **46(10)**: 1177–1201.

Peron H, Delenne JY, Laloui L and El Youssoufi MS (2009b) Discrete element modelling of drying shrinkage and cracking of soils. *Computers and Geotechnics* **36(1–2)**: 61–69.

Rodríguez R, Sanchez M, Ledesma A and Lloret A (2007) Experimental and numerical analysis of desiccation of a mining waste. *Canadian Geotechnical Journal* **44(6)**: 644–658.

Santanach CE, Chabert F, Dunstan DE and Franks GV (2007) Avoiding 'mud' cracks during drying of thin films from aqueous colloidal suspensions. *Journal of Colloid and Interface Science* **313(1)**: 160–168.

Shannon B, Gallage C and Kodikara J (2010) Experimental modelling of coupled water flow and associated movements in swelling soils. In *Proceedings of the 3rd International Conference on Problematic Soils, Adelaide, Australia*, pp. 7–9.

Shinde SB, Uday KV, Kadali S, Tirumkudulu MS and Singh DN (2012) A novel methodology for measuring the tensile strength of expansive clays. *Geomechanics and Geoengineering* **7(1)**: 15–25.

Shokri N and Or D (2013) Drying patterns of porous media containing wettability contrasts. *Journal of Colloid and Interface Science* **391**: 135–141.

Shokri N and Sahimi M (2012) Structure of drying fronts in three-dimensional porous media. *Physical Review E* **85(6)**: article 66312.

Shokri N, Zhou P and Keshmiri A (2015) Patterns of desiccation cracks in saline bentonite layers. *Transport in Porous Media* **110(2)**: 333–344.

Sima J, Jiang M and Zhou C (2014) Numerical simulation of desiccation cracking in a thin clay layer using 3D discrete element modeling. *Computers and Geotechnics* **56**: 168–180.

Singh KB and Tirumkudulu MS (2007) Cracking in drying colloidal films. *Physical Review Letters* **98(21)**: article 218302.

Stirling RA, Hughes P, Davie CT and Glendinning S (2015) Tensile behaviour of unsaturated compacted clay soils – a direct assessment method. *Applied Clay Science* **112–113**: 123–133.

Tang C, Shi B, Liu C, Zhao L and Wang B (2008) Influencing factors of geometrical structure of surface shrinkage cracks in clayey soils. *Engineering Geology* **101(3–4)**: 204–217.

Tang CS, Cui YJ, Tang AM and Shi B (2010) Experiment evidence on the temperature dependence of desiccation cracking behavior of clayey soils. *Engineering Geology* **114(3–4)**: 261–266.

Tang CS, Cui YJ, Shi B, Tang AM and Liu C (2011a) Desiccation and cracking behaviour of clay layer from slurry state under wetting–drying cycles. *Geoderma* **166(1)**: 111–118.

Tang CS, Shi B, Liu C, Suo WB and Gao L (2011b) Experimental characterization of shrinkage and desiccation cracking in thin clay layer. *Applied Clay Science* **52(1)**: 69–77.

Tang CS, Shi B, Liu C, Gao L and Inyang HI (2011c) Experimental investigation of the desiccation cracking behavior of soil layers during drying. *Journal of Materials in Civil Engineering* **23(6)**: 873–878.

Tollenaar RN, van Paassen LA and Jommi C (2017) Observations on the desiccation and cracking of clay layers. *Engineering Geology* **230**: 23–31.

Trabelsi H, Jamei M, Zenzri H and Olivella S (2012) Crack patterns in clayey soils: experiments and modeling. *International Journal for Numerical and Analytical Methods in Geomechanics* **36(11)**: 1410–1433.

Uday KV and Singh DN (2013a) Application of laser microscopy for studying crack characteristics of fine-grained soils. *Geotechnical Testing Journal* **36(1)**: 146–154.

Uday KV and Singh DN (2013b) Investigation on cracking characteristics of fine-grained soils under varied environmental conditions. *Drying Technology* **31(11)**: 1255–1266.

Uday KV, Prathyusha JNV, Singh DN and Apte PR (2015) Application of the Taguchi method in establishing criticality of parameters that influence cracking characteristics of fine-grained soils. *Drying Technology* **33(9)**: 1138–1149.

Vogel HJ, Hoffmann H, Leopold A and Roth K (2005) Studies of crack dynamics in clay soil: II. A physically based model for crack formation. *Geoderma* **125(3–4)**: 213–223.

Wang JJ, Zhu JG, Chiu CF and Zhang H (2007) Experimental study on fracture toughness and tensile strength of a clay. *Engineering Geology* **94(1–2)**: 65–75.

Wang ZJ, Wang H and Cates ME (2001) Effective elastic properties of solid clays. *728 Geophysics* **66(2)**: 428–440.

Xia ZC and Hutchinson JW (2000) Crack patterns in thin films. *Journal of the Mechanics and Physics of Solids* **48(6)**: 1107–1131.

Xu X, Wu S, Jin A and Gao Y (2018) Review of the relationships between crack initiation stress, mode I fracture toughness and tensile strength of geo-materials. *International Journal of Geomechanics* **18(10)**: article 04018136, https://doi.org/10.1061/(ASCE)GM.1943.

Yesiller N, Miller CJ, Inci G and Yaldo K (2000) Desiccation and cracking behavior of three compacted landfill liner soils. *Engineering Geology* **57(1–2)**: 105–121.

Zhang XD, Chen YG, Ye WM *et al.* (2017) Effect of salt concentration on desiccation cracking behavior of GMZ bentonite. *Environmental Earth Sciences* **76(15)**: 1–10.

How can you contribute?

To discuss this paper, please submit up to 500 words to the editor at journals@ice.org.uk. Your contribution will be forwarded to the author(s) for a reply and, if considered appropriate by the editorial board, it will be published as a discussion in a future issue of the journal.